Acta Materialia 195 (2020) 541–554

Contents lists available at ScienceDirect

Acta Materialia

journal homepage: www.elsevier.com/locate/actamat

Full length article

Age-hardening response of AlMgZn alloys with Cu and Ag additions

Lukas Stemper[a,*], Matheus A. Tunes[b], Paul Oberhauser[c], Peter J. Uggowitzer[b], Stefan Pogatscher[a,b,**]

[a] Christian Doppler Laboratory for Advanced Aluminum Alloys, Chair of Nonferrous Metallurgy, Montanuniversitaet Leoben, Franz-Josef-Straße 18, 8700 Leoben, Austria
[b] Chair of Nonferrous Metallurgy, Montanuniversitaet Leoben, Franz-Josef-Straße 18, 8700 Leoben, Austria
[c] AMAG rolling GmbH, Lamprechtshausener Str. 61, 5282 Ranshofen, Austria

ARTICLE INFO

Article history:
Received 6 March 2020
Revised 27 May 2020
Accepted 30 May 2020
Available online 5 June 2020

Keywords:
Aluminum alloys
AlMg alloys
Alloy design
Hardening behavior
Precipitation

ABSTRACT

A recurrent challenge with aluminum alloys is their longstanding trade-off between mechanical strength and formability. Recently recyclability has put further pressure on the development of single-alloy concepts for solving this challenge. This study addresses an AlMg-based system featuring additional elements to facilitate age-hardening but retaining a high Mg content for inherent pronounced strain hardening as a potential candidate. Age-hardening was enabled by T-phase based precipitation in the commercial alloy EN AW-5182 via the addition of 3.5 wt.% of Zn. The investigation shows that minor additions of Cu and Ag enhance and accelerate it. The study also compares single-step and double-step artificial aging. Hardness and tensile testing and scanning transmission electron microscopy methods were deployed to characterize the alloys investigated, mechanically and microstructurally. An alloy with added Zn, Cu and Ag showed improved strain hardening and reduced serrated flow in the soft state, while exhibiting an age-hardening response of up to 326 MPa in yield strength leading to an ultimate tensile strength of 550 MPa in peak-aged condition. The study discusses the evolution of the microstructure during artificial aging in the light of Zn, Cu and Ag additions and their effect on the precipitation process.

1. Introduction

In recent decades CO_2 emissions have been significantly boosted by the accelerated development of the traffic and transportation sectors, generating harmful changes in the global climate [1,2]. Increasing political awareness and rising economic importance have triggered the development of new and sustainable materials as solutions to meet this challenge. Deploying low-density alloys such as aluminum alloys in lightweight construction design is a well-known weight reduction approach to curbing emissions.

Unfortunately, multiple operational requirements and engineering criteria, in particular those which promote strength and ductility, require the utilization of several different alloying concepts and therefore limit the recyclability at the end of a product's lifetime [3].

A promising approach to this problem is to establish a single-alloy concept which combines desirable material properties and easy recyclability. The automotive industry, in particular, has tried to do this using AlMgSi alloys (6xxx). Here suitable hardening potential and corrosion resistance have been achieved, but the requirements for complex forming operations remain unfulfilled.

Commercial AlMg alloys (5xxx), by contrast, exhibit a high level of uniform elongation and work hardenability [4]. This makes them beneficial in complex forming operations. However, surface deterioration via formation of stretcher strains [5,6] and undesired strength reduction during room temperature storage [7] and paint bake treatment [8] limit their application.

Several attempts have been made to overcome these challenges. Modification with targeted amounts of Zn has produced alterations in the precipitation sequence to favor T-phase formation [$Mg_{32}(Al,Zn)_{49}$] [9], resulting in increased strength [10–13], delayed onset of serrated flow [11,14,15] and improved intergranular corrosion resistance (IGC) [10,16–18]. Adding Cu has been shown

* Corresponding author.
** Corresponding author at: Christian Doppler Laboratory for Advanced Aluminum Alloys, Chair of Nonferrous Metallurgy, Montanuniversitaet Leoben, Franz-Josef-Straße 18, 8700 Leoben, Austria.
E-mail addresses: lukas.stemper@unileoben.ac.at (L. Stemper), stefan.pogatscher@unileoben.ac.at (S. Pogatscher).

https://doi.org/10.1016/j.actamat.2020.05.066
1359-6454/

Table 1
Main nominal element content of the alloys investigated in wt.%.

	Mg	Mn	Zn	Cu	Ag
Alloy Zn	4.7	0.4	3.5	–	–
Alloy Zn Ag	4.7	0.4	3.5	–	0.17
Alloy Zn Cu0.15	4.7	0.4	3.5	0.15	–
Alloy Zn Cu0.15 Ag	4.7	0.4	3.5	0.15	0.17
Alloy Zn Cu0.5	4.7	0.4	3.5	0.5	–
Alloy Zn Cu0.5 Ag	4.7	0.4	3.5	0.5	0.17

to reduce [19] or even compensate [20–22] for softening during paint bake treatment, because the Cu additions generate potential for precipitation hardening by S-phase [Al_2MgCu] and its precursors [23–26]. Applying minor amounts of Ag is also a well-known way to enhance the age hardening response in AlCuMg [27,28] and AlZnMg [29–31] alloys by modifying the precipitation sequence. This has been also reported for Ag-doped AlMg [32,33] and AlMgCu [34–36] alloys, where the hardening response has been attributed to icosahedral quasi-crystals which tend to develop in the T- or Z-phases.

The combined addition of Zn and Cu in AlMg alloys has attracted increasing attention in the past few years due to these alloys' positive effect on stress corrosion cracking [37–39] and on the hardening response during artificial aging. Cao et al. [40–42] and Hou et al. [43,44] focused their investigations on plate-like material and showed that the precipitation sequence in these alloys depends strongly on thermal treatment. They found that peak hardness is generated by synergistic effects between T- and S-phase after single-step artificial aging, but by the Cu-incorporated T-phase if a pre-aging treatment was applied. Recent work by some of the present authors on high pressure die casting alloys with similar compositions has supported these findings [45].

The modified 5xxx series may thus be a potential route to a single-alloy concept which both offers high strength and formability and addresses the challenges of mass reduction and multi-alloy recyclability. The aim of this study is to evaluate the eligibility of Zn-modified EN AW-5182 alloy with Cu additions for this purpose, especially in terms of hardening potential. Here the use of Ag as a minor alloying element and thermal treatment design are special focuses. The influence of alloy composition on the development of microstructure during artificial aging treatment is discussed in detail.

2. Experimental

Table 1 shows the main element content of the alloys investigated. All alloys are based on EN AW-5182 as supplied by AMAG rolling GmbH, modified by adding Zn and varying amounts of Cu and Ag.

All alloys were melted and cast as laboratory scaled slabs using a laboratory scale vacuum induction furnace. A detailed description of alloy production and processing can be found elsewhere [46]. Two-step-homogenization of the slabs before hot rolling (465 °C) was performed for 24 h at 460 °C and 470 °C. Hardness testing samples and tensile testing samples were cold rolled to a final thickness of 2 mm and 1.2 mm to ensure cold rolling degrees of 50% and 20%, respectively. To generate a supersaturated solid solution, all samples were solution heat treated at 465 °C for 35 min and quenched by immersion in water at room temperature. Artificial aging was performed in a circulating oil bath at 125 °C and 100 °C/3 h + 175 °C for single-step and double-step aging treatment, respectively.

Hardness testing was performed on an EMCO-TEST M4 unit according to Brinell's method (HBW 2.5/62.5) while tensile testing was done on a Zwick-Roell tensile testing unit BT1-FR100THW.A2K equipped with a 50 kN load cell. The graphed data represent an average of five and three independent hardness and tensile testing measurements, respectively.

Thin-foils for scanning transmission electron microscopy (STEM) were punched out of sheets and ground to a thickness of 100 µm. Twin jet electro-polishing was performed using a solution of 75% methanol and 25% nitric acid, a temperature of −10 °C and an electric potential of 10 V. Diffraction patterns (DP) and energy dispersive x-ray spectroscopy (EDS) measurements were carried out with a Thermo Fisher Scientific™ Talos F200X scanning transmission electron microscope.

3. Results

3.1. Screening of the hardening potential

3.1.1. Effect of Cu and Ag on single-step aging

Fig. 1 shows the evolution of the hardness of the investigated alloys during single-step aging at 125 °C. We first consider the Ag-free alloys (full lines). While the Cu-free alloy (Alloy Zn; red line) responds to the aging treatment only after extended aging time, adding Cu shifts the hardening onset to earlier times. This is more pronounced in the variant containing a large amount of Cu (Alloy Zn Cu0.5; orange line), compared to the alloy containing a medium amount of Cu (Alloy Zn Cu0.15; blue line), where this effect is only minor. It is interesting to note that Alloy Zn Cu0.5 exhibits a steady hardness increase immediately at the beginning of aging, while alloys with no or minor Cu addition show a relatively sharp transition between low and high hardness levels. Nevertheless, the maximum hardness observed exhibits only minor differences over the investigated time range, independent of the Cu content. Small additions of Ag (dashed lines) significantly accelerate the hardening response and exceed the top hardness level of the non-Ag-doped alloys (full lines) by approximately 25 HBW on average, reaching a maximum hardness of 166 HBW in Alloy Zn Cu0.5 Ag.

3.1.2. Effect of Cu and Ag on double-step aging

Besides adding minor alloying elements to enhance and accelerate hardening, applying a pre-aging treatment is reported to have accelerating effects. Inspired by earlier findings [45], all alloys investigated were pre-aged at 100 °C for 3 h before aging at higher temperature (175 °C). The hardness evolution of the second aging step is shown in Fig. 2 for non-Ag-doped (full lines) and Ag-doped (dashed lines) samples of Alloy Zn (red curves), Alloy Zn Cu0.15 (blue curves) and Alloy Zn Cu0.5 (orange curves).

After pre-aging of the non-Ag-doped alloys the initial hardness in the second aging stage increases proportionally to the Cu content. Both the hardening onset and the peak hardness are shifted to markedly earlier aging times (9 h instead of 9 days), resulting also in early over-aging when compared to single-step aging. The peak hardness follows the same trend as the initial hardness and exhibits higher levels compared to single-step-aged samples except Alloy Zn.

Alloy samples containing Ag exhibit a higher initial hardness level after pre-aging compared to the non-Ag-doped samples, which tends to drop at the beginning of the second aging stage before an accelerated increase to peak hardness takes place. The accelerating effect of Ag diminishes with increasing Cu content but Ag still promotes a slightly higher overall hardness, especially in peak-aged condition.

The maximum hardness found for all Ag-containing alloys during double-step aging is slightly lower than their maximum hardness found during single-step aging (6% in average). However, peak-aging time is reduced by a factor of ~18 if double-step aging was applied.

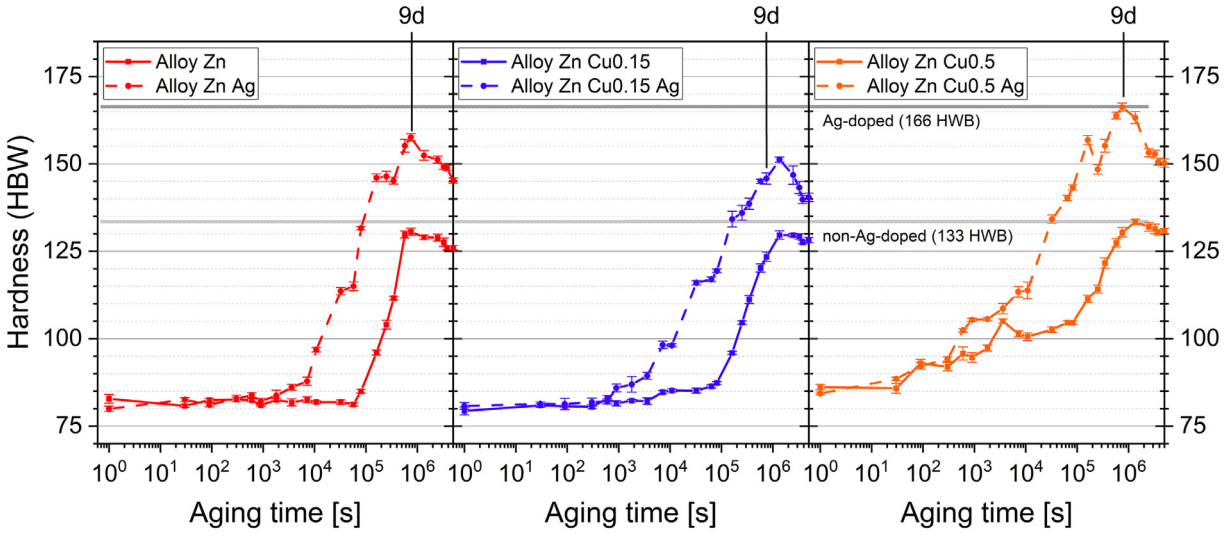

Fig. 1. Hardening curves of Alloy Zn (red lines), Alloy Zn Cu0.15 (blue lines) and Alloy Zn Cu0.5 (orange lines) for single-step artificial aging at 125 °C; dashed lines refer to the corresponding Ag-doped alloys.

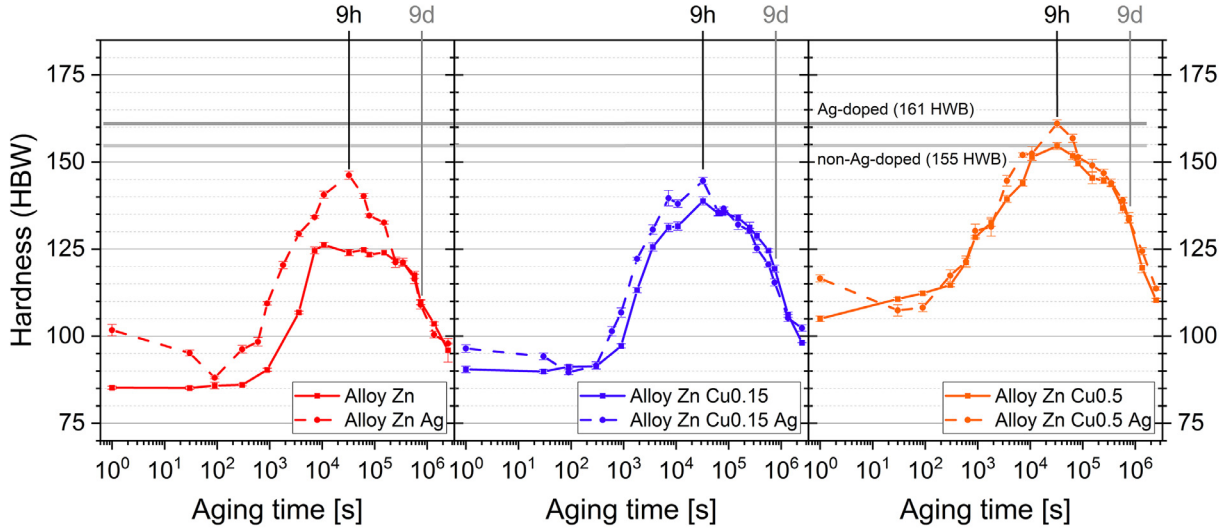

Fig. 2. Hardening curves of Alloy Zn (red lines), Alloy Zn Cu0.15 (blue lines) and Alloy Zn Cu0.5 (orange lines) for the second stage of double-step artificial aging (100 °C/3 h + 175 °C/x); dashed lines refer to the corresponding Ag-doped alloys. For comparison the peak-aging time for single-step aging from Fig. 1 is also indicated (9d).

3.2. Effect of increasing the alloy content

For alloys containing both Cu and Ag, the boosting effect of each additional alloying element seems to accumulate in step with the other (see Fig. 3), especially for single-step aging (Fig. 3a), which generates the highest level of hardness observed in this study. To understand and characterize this observation, further investigation will focus on Alloy Zn (unbroken red line), Alloy Zn Cu0.5 (dashed blue line) and Alloy Zn Cu0.5 Ag (dotted orange line) to evaluate the effect of a gradual increase in total alloy content.

3.2.1. Hardness evolution

3.2.1.1. Single-step aging (125 °C). After solution heat treatment and quenching (condition A in Fig. 3a) all the supersaturated alloys exhibit a similar hardness of approximately 85 HBW. After only 3 h of aging at 125 °C (marked as condition B in Fig. 3a) Alloy Zn Cu0.5 and Alloy Zn Cu0.5 Ag have already gained a distinct hardness increases of 15 and 30 HBW, respectively, while for Alloy Zn no increase in hardness is observed. Peak hardness (marked as condition C in Fig. 3a) is reached after 9 days of aging for Alloy Zn and Alloy Zn Cu0.5 Ag and after 16 days for Alloy Zn Cu0.5. While Cu-additions exhibit an only minor benefit on peak hardness, the combined addition of Cu and Ag promotes a maximization of hardness reaching 166 HBW.

With extended aging time the hardness of all three alloys starts to decrease (over-aging) but remains on a high level also for longer aging times (45 days).

3.2.1.2. Double-step aging (100 °C/3 h + 175 °C). After the first aging stage (condition E in Fig. 3b) Alloy Zn Cu0.5 and Alloy Zn Cu0.5 Ag exhibit already a significant hardening response, while no increase can be observed in Alloy Zn. This trend is consistent with condition B in Fig. 3a.

Peak hardness was reached after 9 h of second-step aging (condition F in Fig. 3b). While both Cu-containing alloys show a more or less distinct climax Alloy Zn exhibits a hardness plateau. It is also interesting to note that peak hardness of Alloy Zn and Alloy Zn Cu0.5 Ag observed in single-step aging could not be reached if double-step aging was applied. In contrast peak hardness of Alloy Zn Cu0.5 is significantly higher and almost at the same level of the Ag-containing alloy. After 16 days of aging (condition G in

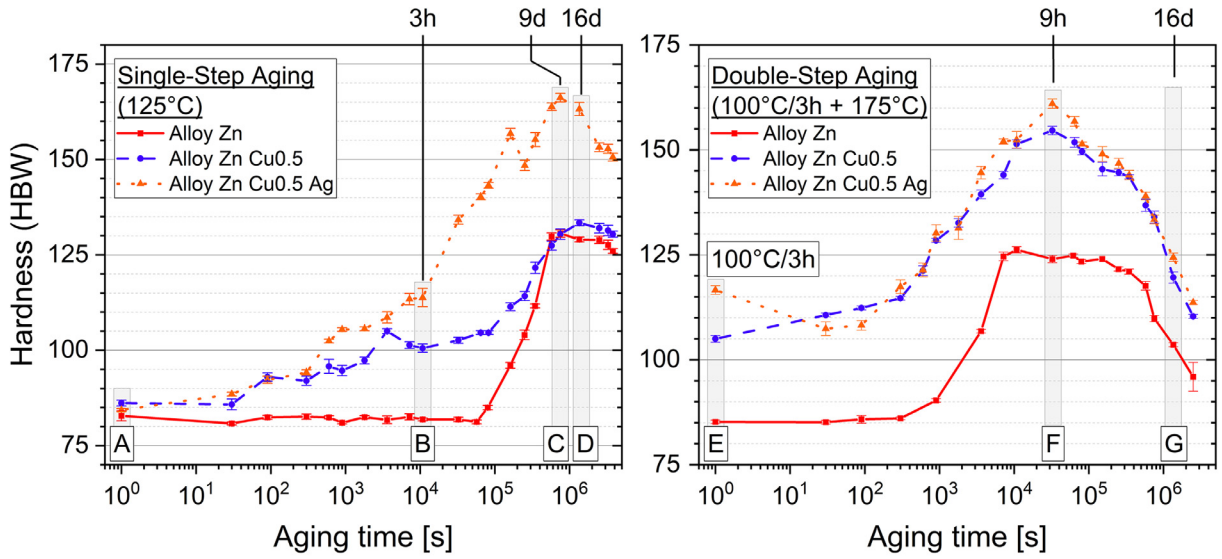

Fig. 3. Comparison of the hardening curves of Alloy Zn (unbroken red line), Alloy Zn Cu0.5 (dashed blue line) and Alloy Zn Cu0.5 Ag (dotted orange line) (a) for single-step aging (b) for double-step aging. *A* = as-quenched condition, B, C, D, E, F and *G* = conditions of microstructure investigation.

Fig. 3b) all three alloys show decreased hardness due to distinct over-aging.

3.2.2. Microstructural evolution

To understand the effect of alloy composition on the observed hardening response, detailed investigations into the evolution of the microstructure with progressing artificial aging time were conducted in the form of diffraction studies and EDS measurements. For under-aged conditions bright field (BF) images were additionally acquired.

According to literature [40,43] and thermodynamic calculations [47,48], hardening by T- and/or S-phase, including precursors, seems to be the most reasonable mechanism.

In equilibrium condition the S-phase (Al_2MgCu) is expected to exhibit an orthorhombic structure (a_S = 0.400 nm, b_S = 0.923 nm and c_S = 0.714 nm), while the T-phase shows a cubic structure (a_T = 1.416 nm, b_T = 1.416 nm, c_T = 1.416 nm) [23,49,50].

Both phases can be identified according to their distinct reflection spots within the aluminum matrix along the ⟨001⟩ zone axis, exposing the characteristic T-phase spots at the 2/5 and 3/5 ⟨022⟩Al position and the characteristic S-phase spots between the {002}Al and {022}Al spots, respectively [42]. In view of the similar crystal structure reported for precursors and equilibrium phases, they were not distinguished in this study [9,26,51,52].

It is worth emphasizing that microstructural investigations on under-aged and long-aged conditions were conducted after similar aging time for single-step and double-step aging for comparison reasons. Peak-aged conditions were derived from hardening curves of Alloy Zn Cu0.5 Ag for each treatment strategy individually.

3.2.2.1. Single-step aging. Figs. 4 and 5 show the BF images, DPs and selected EDS mappings of Alloy Zn (a), Alloy Zn Cu0.5 (b) and Alloy Zn Cu0.5 Ag (c) after 3 hours of aging at 125 °C, corresponding to the under-aged condition B in Fig. 3a.

In contrast to Alloy Zn (Fig. 4a) dark spots are evident beside dispersoids in the BF images of both Alloy Zn Cu0.5 and Alloy Zn Cu0.5 Ag (Fig. 4b and c) but with a higher number density in the Ag-containing alloy.

Over- and under-focusing the BF images did not change the Fresnel contrast of the dark spots, which indicates that they are most probable neither electron-beam generated voids nor dislocation loops. Taking the increased hardness levels of Alloy Zn Cu0.5 and Alloy Zn Cu0.5 Ag and the absence of extra reflection spots beside the matrix spots in the corresponding DPs (Fig. 5) into account, it is reasonable to identify these dark spots as precursors of hardening precipitates, most likely GPI-zones according to the nomenclature proposed by Hou et al. [43] and electron-beam contrast mechanisms presented in textbooks [53,54].

In contrast to the findings in the BF images EDS mappings revealed no distinct aggregation of hardening elements (Fig. 5) at any magnification investigated. This method might be inappropriate at this condition due to its detection limit in combination with the very likely dissolution of the highly unstable precursors by electron irradiation introduced during the measurement itself, especially at higher magnification.

Subsequent aging to peak hardness (condition C in Fig. 3a) generates the microstructures shown in Fig. 6. A clear aggregation of the hardening elements Mg and Zn can be observed for all three alloys. Extra reflection spots in the DPs corresponding to T-phase (or its precursors) indicate that the precipitates have developed a distinct crystal structure under the condition studied. It should also be noted here that no distinction was made in this study between the precursor and the equilibrium phase. Alloy Zn Cu0.5 (Fig. 6b) exhibits additional reflections corresponding to S-phase or its precursors (inset) but a clear aggregation of Mg and Cu related to S-phase formation was not observed which may be related to their low number density implied by the weak expression of the Bragg diffraction signal. Interestingly also a distinct aggregation of Cu with Mg and Zn was found neither in Alloy Zn Cu0.5 nor in Alloy Zn Cu0.5 Ag (white circles in Fig. 6b and d) but a significant aggregation of Mg and Zn with Ag (green circles in Fig. 6d) is evident in the latter alloy. Note that for Alloy Zn Cu0.5 the Cu signal is disturbed by anodic depositions of Cu-rings formed during electro-polishing (Cu mapping in Fig. 6b) [55].

The hardening phases in the non-Ag containing alloys exhibit a similar distribution and density in the matrix, while the microstructure of Alloy Zn Cu0.5 Ag contains of significantly finer precipitates in a higher density. This observation agrees with the findings of hardness measurements and indicates that Ag atoms have a strong influence on the initial formation of GPI-zones.

The influence of alloy composition on microstructural features is most pronounced in the long-aged condition (condition D in Fig. 3a) and is shown in Fig. 7. Adding Cu seems to change the morphology of the hardening precipitates from an elongated, lath-

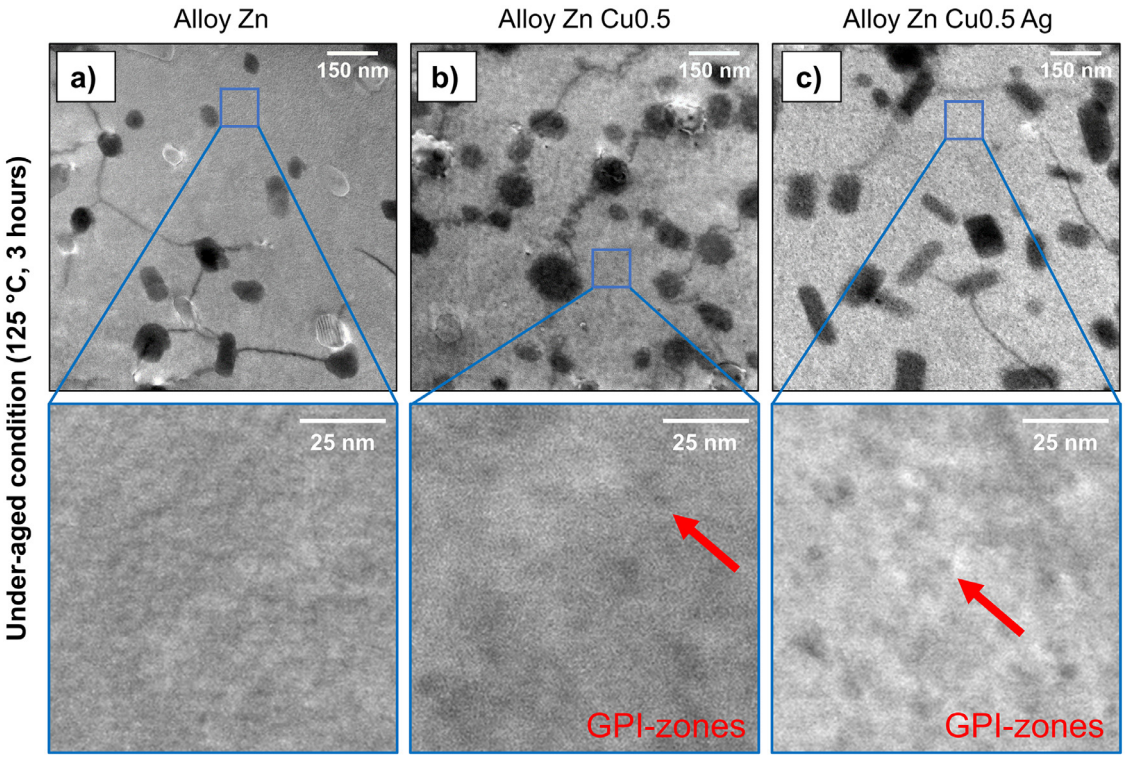

Fig. 4. BF images of Alloy Zn (a), Alloy Zn Cu0.5 (b) and Alloy Zn Cu0.5 Ag in under-aged condition (125 °C/3 h). Red arrow indicates a GPI-zone representatively.

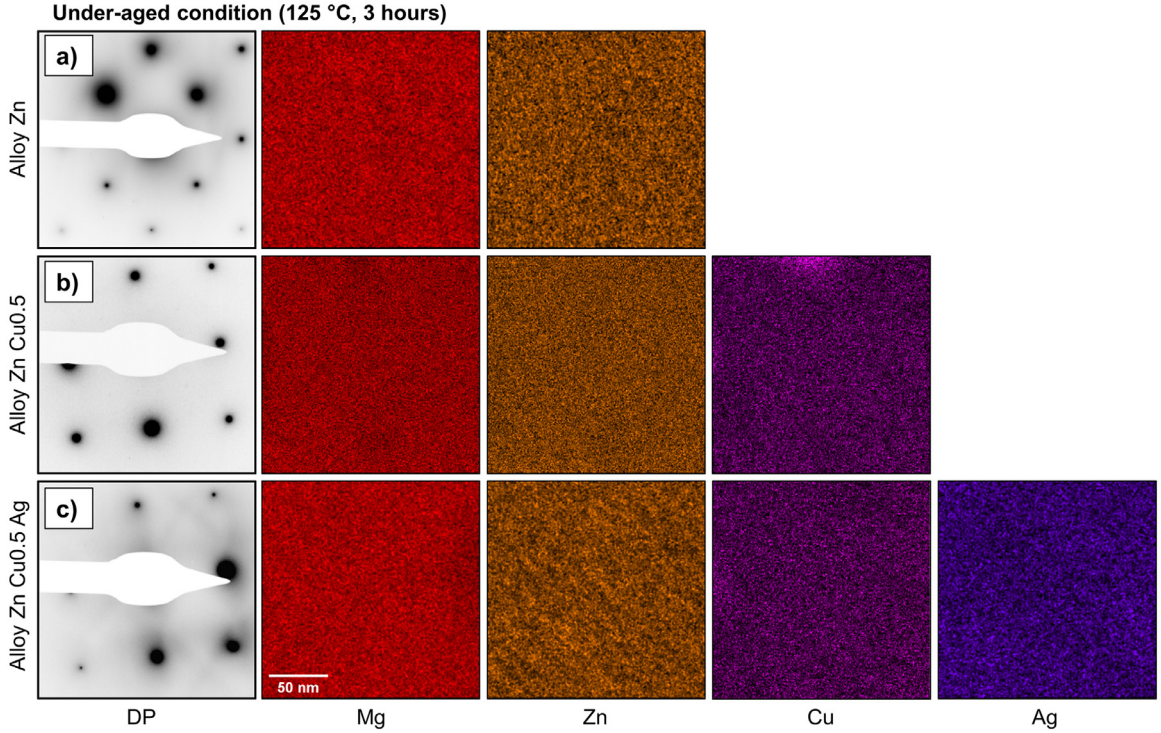

Fig. 5. DPs and EDS mappings of the main alloying elements in Alloy Zn (a), Alloy Zn Cu0.5 (b) and Alloy Zn Cu0.5 Ag (c) in under-aged condition (125 °C/3 h). The scale bar in the Mg mapping in (c) applies to all EDS mappings.

like shape in Alloy Zn (Fig. 7a) to a more spherical shape in Alloy Zn Cu0.5 (Fig. 7b). This effect may be related to the progression of hardness, because Alloy Zn Cu0.5 has only reached now peak hardness at this stage, while a hardness decrease due to over-aging is already noticeable for Alloy Zn. Again, anodic depositions in Alloy Zn Cu0.5 are present in the EDS mapping and distinct aggregation of Cu with Mg (S-phase) or with Mg and Zn (Cu-containing T-phase) is unclear (white circles in Fig. 7b). In contrast to Alloy Zn and Alloy Zn Cu0.5, for which the supersaturation of Mg and Zn within the Al matrix has drastically decreased via the formation of precipitates, this effect is observed for the Ag-containing alloy only to a minor extent. The precipitation density in Alloy Zn Cu0.5 Ag is

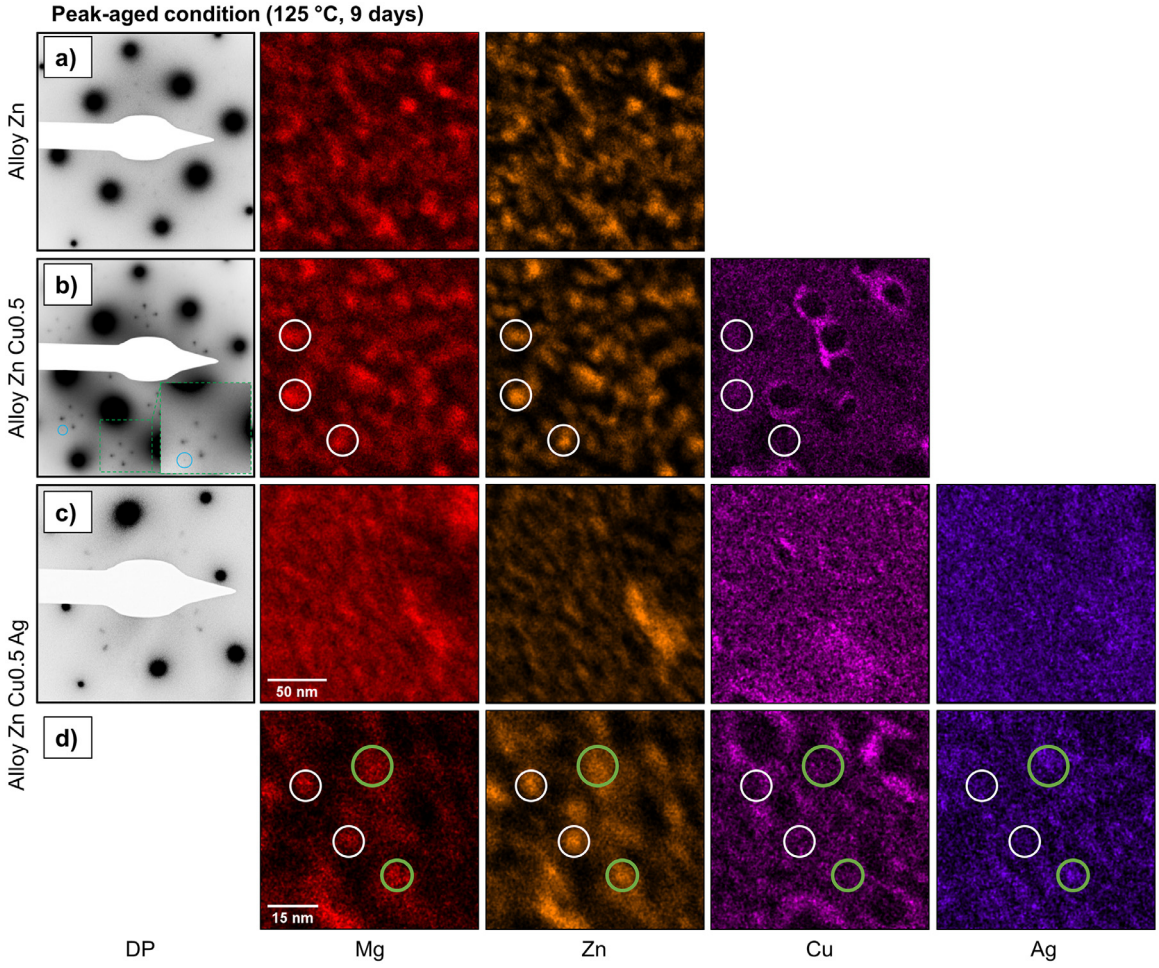

Fig. 6. DPs of the alloys and EDS mappings of the main alloying elements in Alloy Zn (a), Alloy Zn Cu0.5 (b) and Alloy Zn Cu0.5 Ag (c) in peak-aged condition (125 °C/9 days). Extra reflection spots marked by blue circles in DP of b) correspond to S-phase. White circles indicate correlation of only Mg and Zn, green circles indicate aggregation of Mg, Zn and Ag. The scale bar in the Mg mapping in (c) applies to all EDS mappings in (a), (b) and (c), the scale bar in the Mg mapping in (d) applies to all EDS mappings in (d).

significantly higher, which correlates well with the higher hardness level found. Interestingly, at this stage the Ag-added alloy (Fig. 7c and Fig. 7d) exhibits also aggregates of Mg and Ag with minor Zn content (green circles) as well as Mg-Zn-Ag aggregates with significant Cu-incorporations (orange circles) beside Mg-Zn aggregates without enrichment of Cu and Ag (white circles). As expected, the DPs show the same reflection spots as observed in the peak-aged state, although they are more pronounced in the long-aged condition.

3.2.2.2. Double-step aging. The under-aged condition for the double-step aging strategy corresponds to the initial state of the second aging step (3 hours at 100 °C, condition E in Fig. 3b). The BF images of the investigated alloys in this state are shown in Fig. 8, the corresponding DPs and selected EDS mappings are depicted in Fig. 9.

Alloy Zn Cu0.5 (Fig. 8b) and Alloy Zn Cu0.5 Ag (Fig. 8c) exhibit a high number density of finely dispersed dark spots, identified as hardening precursors (GPI-zones) in the same way already mentioned before. The BF image of Alloy Zn (Fig. 8a) in contrast shows fainted dark spots in a low number density and a significantly lower contrast. Due to the absence of any hardening response in the corresponding alloy they are assumed to be solute aggregates, which have not developed into GPI-zones at this stage.

Findings in the BF images are supported by the DPs in Fig. 9 due to the fact that only matrix reflection spots can be observed in any investigated alloy. EDS mappings in the same figure might indicate a certain level of solute aggregation (when compared to Fig. 5) but that can't be taken to be significant for the reasons already mentioned.

Fig. 10 shows the DPs and selected EDS mappings for each alloy after aging to peak hardness in the second aging stage (condition G in Fig. 3b). The distinct aggregation of Mg and Zn and the extra reflection spots beside the matrix spots clearly identify the hardening precipitates as T-phase.

While large needle-like precipitates in low number density are present in Alloy Zn (Fig. 10a), finely dispersed globular precipitates exist in high number density in Alloy Zn Cu0.5 (Fig. 10b) and Alloy Zn Cu0.5 Ag (Fig. 10c). Only minor differences can be observed between the latter two which is consistent with the only minor deviations in measured hardness. Even though the EDS signal of Cu shows slight enrichment in Mg-Zn aggregates (indicated by white circles) an explicit tendency is hard to see in either Alloy Zn Cu0.5 (Fig. 10b) or Alloy Zn Cu0.5 Ag (Fig. 10c) at this stage but the absence of S-phase spots in the DP of Alloy Zn Cu0.5 might support the aggregation tendency of Mg, Zn and Cu.

After 16 days of aging in the second aging stage (condition G in Fig. 3b) the hardness of the investigated alloys is strongly deteriorated due to undesired precipitate growth as shown in Fig. 11. Extra reflection spots of T-phase are evident in the DPs of Alloy Zn (a), Alloy Zn Cu0.5 (b) and Alloy Zn Cu0.5 Ag (c). The size of the already large precipitates observed in Alloy Zn in

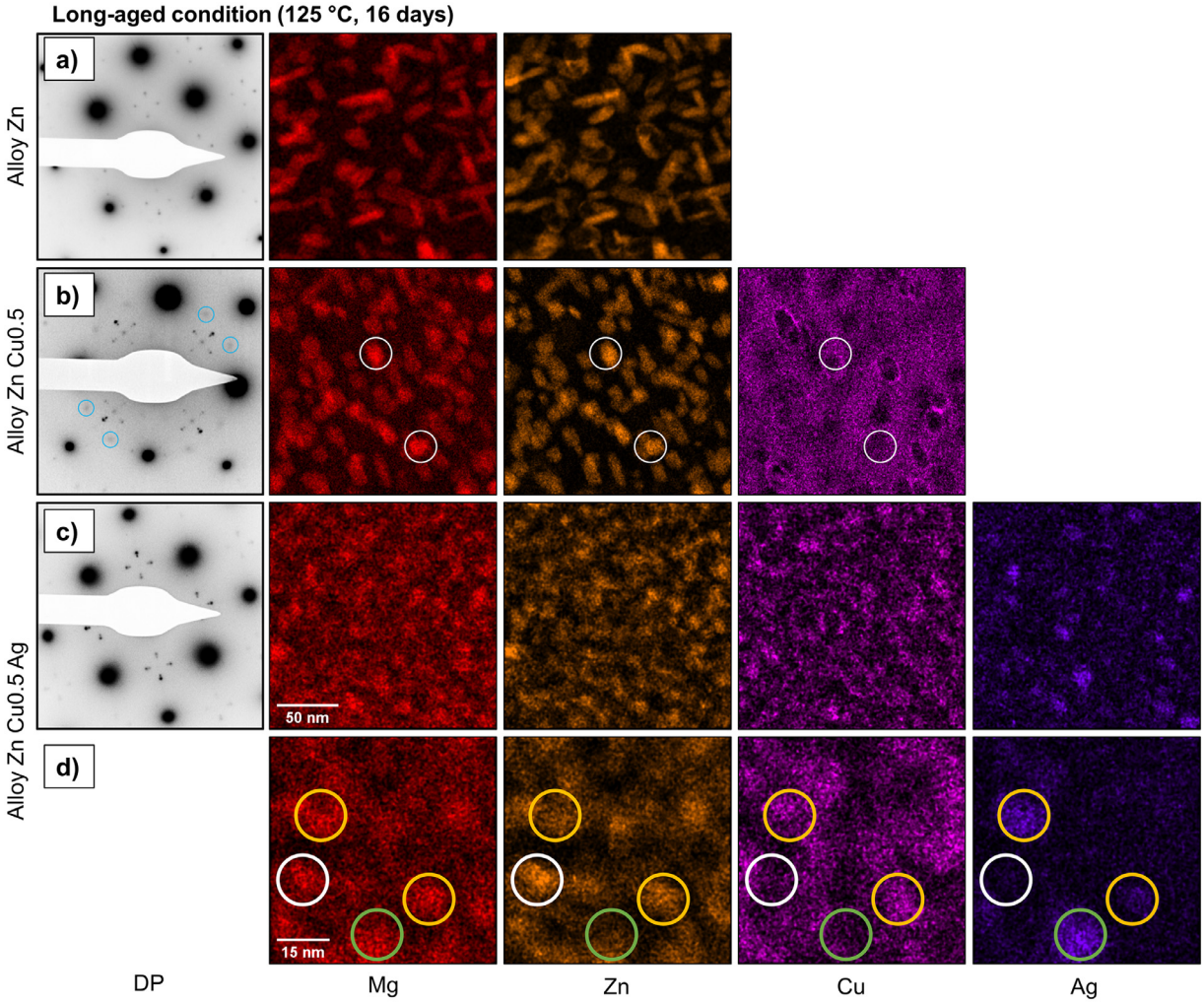

Fig. 7. DPs of the alloys and EDS mappings of the main alloying elements in Alloy Zn (a), Alloy Zn Cu0.5 (b) and Alloy Zn Cu0.5 Ag (c) in long-aged condition (125 °C/16 days). Extra reflection spots marked by blue circles in DP of b) correspond to S-phase White circles indicate correlation of only Mg and Zn, green circles indicate aggregation of Mg, Zn and Ag and orange circles highlight correlation of Mg-Zn-Cu-Ag. The scale bar in the Mg mapping in (c) applies to all EDS mappings in (a), (b) and (c), the scale bar in the Mg mapping in (d) applies to all EDS mappings in (d).

peak-aged condition (Fig. 10a) has even increased to over 100 nm in long-aged condition (Fig. 11a) resulting in a strong decrease of number density. Precipitates in Alloy Zn Cu0.5 (Fig. 11b) and Alloy Zn Cu0.5 Ag (Fig. 11c) have also coarsened and a decrease in number density is also evident at this stage compared to peak-condition (Fig. 10b and c), but in contrast to the non-Cu-containing alloy, the fraction, size and distribution of the particles still accounts for the higher hardness levels observed.

At this aging stage small precipitates with a clear enrichment of Cu (red circles) can be observed beside large Mg-Zn aggregates without Cu (white circles) in Alloy Zn Cu0.5 (Fig. 11b). In the Ag-containing alloy (Fig. 11c) most of the particles contain significant amounts of Cu (red circles) with some of them additionally enriched with Ag (orange circles).

3.3. Mechanical properties

To evaluate the full strengthening potential of such alloys, tensile testing was performed for the most promising one in terms of its hardening response (Alloy Zn Cu0.5 Ag) in the as-quenched state (condition A in Fig. 3a) and at its maximum hardness (condition C in Fig. 3a). While the as-quenched samples (curve A in Fig. 12) exhibit high fracture elongation, low yield strength (143 MPa) and excellent work hardenability, the peak-aged state (curve C in Fig. 12), offers a high yield strength of 469 MPa which corresponds to a dramatic gain in strength of 326 MPa (~330%). Nevertheless, the peak-aged state still retains a significant strain hardening potential, which leads to an ultimate tensile strength of 550 MPa. The remaining fracture elongation is 9.3%. Moreover, no serrated flow caused by the PLC-effect is present [15,56] in the peak-aged state. It is worth noting that even in the as-quenched state only a weak PLC-effect can be seen, while the other characteristics of the stress strain curve are highly comparable to the standard EN AW-5182 alloy (gray curve in Fig. 12) which was used as a base in production of the alloys. By plotting the strain hardening rate SHR over true stress (Kocks-Mecking-Plot) for fitted stress-strain curves of EN AW-5182 and Alloy Zn Cu0.5 Ag in soft temper (inset in Fig. 12) a shift to higher SHR and a flattening of the curve for the Zn-Cu-Ag-doped alloy is observed which can be linked to promoted dislocation formation and reduced dislocation annihilation associated with enhanced stretch-formability [57–59].

4. Discussion

Adding Zn to a commercial EN AW-5182 alloy introduces an age hardening potential by enabling T-phase precipitation. Our study showed that this effect can be enhanced and accelerated by adding minor amounts of Cu and Ag. Additionally, tensile testing conducted on Alloy Zn Cu0.5 Ag further gives strong indication

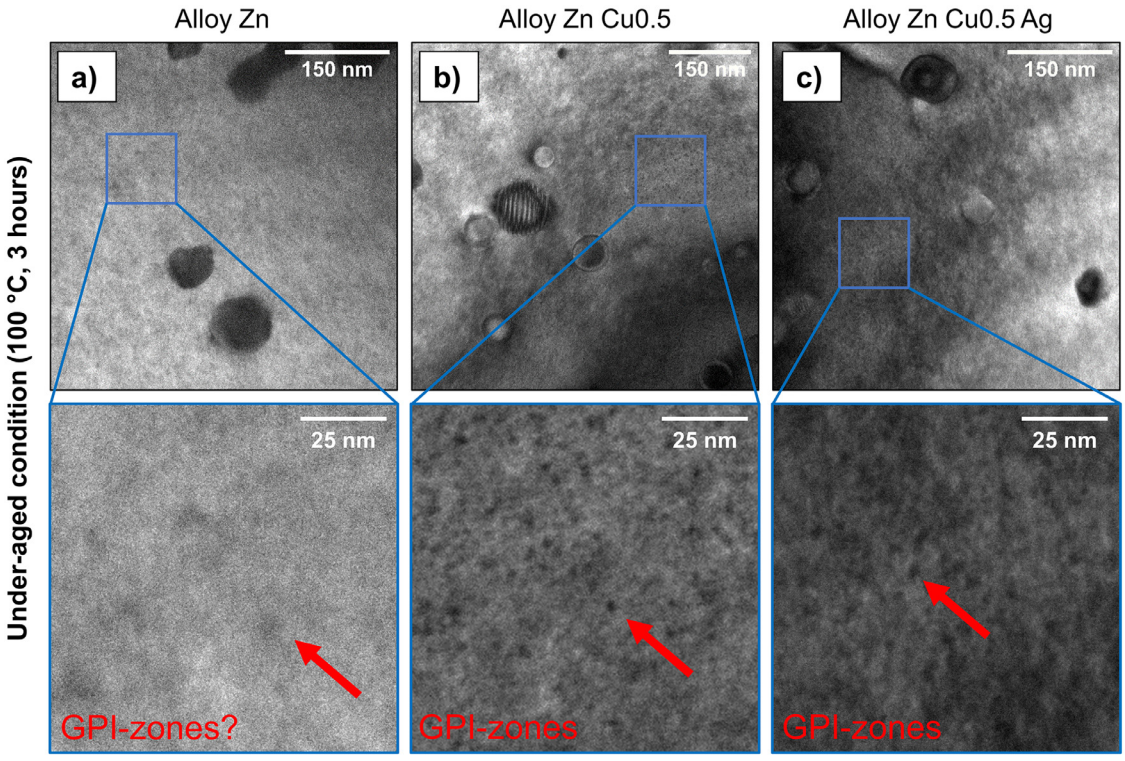

Fig. 8. BF images of Alloy Zn (a), Alloy Zn Cu0.5 (b) and Alloy Zn Cu0.5 Ag in under-aged condition of single-step aging (100 °C/3 hours). Red arrow indicates a GPI-zone representatively.

for improved stretch-formability in the soft condition compared to the EN AW-5182 alloy. The results are discussed with a focus on successive addition of the alloying elements Zn, Cu and Ag to the base alloy.

4.1. Effect of Zn on the aging response of EN AW-5182

According to thermodynamic calculations [47,48] the T-phase ($Mg_{32}(Al,Zn)_{49}$) is supposed to be the dominating hardening phase in this alloy system under equilibrium condition. Hardening by T-phase or its precursor has been reported for 7xxx-series alloys with low Zn/Mg-ratio [13] as well as for modified AlMg alloys [11,12,40], but the exact description of the precipitation sequence is still a matter of debate as it is strongly dependent on the chemical composition of the alloy.

Hou et al. [43,44] recently proposed a precipitation sequence [SSSS (supersaturated solid solution) ➔ GPI zone ➔ GPII zone (intermediate phase T'') ➔ intermediate phase T' ➔ equilibrium phase T-$Mg_{32}(Al,Zn)_{49}$] which includes fully coherent clusters with no diffraction spots (GPI), fully coherent precipitates with diffraction spots (GPII, T''), semi-coherent (T') and incoherent (T) precipitates with diffraction spots. Such a precipitation sequence seems to be the most adequate for the alloy system investigated in this study.

Generally precipitation is governed by two mechanism: the nucleation and growth of precipitates [4,60]. Their nucleation is determined by an advantageous aggregation/formation while their growth is driven by diffusion and attachment of precipitate-forming solutes.

After 3 hours of single-step aging at 125 °C of Alloy Zn, neither an increase in hardness nor GPI-zones in the BF image were found in this under-aged condition (Fig. 4a). EDS mappings for this condition are not taken into account for interpretation due to insufficient detection limit and the radiation damage yield by the measurement itself.

However, our findings correlate well with the results by Cao et al. [40] for an under-aged Zn-containing AlMg alloy. The lower aging temperature applied in the current study facilitates a lower diffusion rate of solutes and generates a shift in the hardening onset to extended aging time, which is attributed to a relatively high activation energy and a larger critical nucleus of the T-phase [52,61]. On the other hand the formation of solute aggregates/GPI-zones is more beneficial at lower temperatures in the Al-Mg-Zn system [52,62]. Based on recent DFT calculations (see Table 2a) we therefore suppose that the microstructure already consists of small, non-hardening Mg-Va/Zn-clusters due to their highest formation probability (highest binding energy) in the Al-Mg-Zn system. These clusters are not detectable with the applied experimental methods but they establish their effect once the barrier of nucleation and growth of T-phase is overcome. Please note that information on the early stages of aging is limited at the moment due to the novelty of the examined alloy systems. More detailed investigations need to be carried out but would go beyond the scope of this study, which is to explore their hardening potential.

STEM investigations on Alloy Zn after prolonged aging time indicate that the hardening observed indeed results from T-phase precipitates or its precursors. They exhibit an elongated, lath-like shape, which is more pronounced in the in long-aged condition than in the peak-aged condition (compare Alloy Zn in Figs. 6a and 7a).

If a pre-aging treatment is applied, indications of GPI-zones in low number density can be found in the under-aged condition of double-step aging of Alloy Zn (Fig. 8a). Even though the limited diffusivity at 100 °C prevents solute attachment and growth of precursors, their formation seems to be favored due to increased Mg-supersaturation and short diffusion pathways [42,45,62]. Upon subsequent high temperature aging (175 °C) precursors formed in first low-temperature stage act as preferential nucleation sites and precipitate growth is facilitated due to enhanced diffusion and at-

Table 2
Binding energies calculated according to DFT for various cluster configurations of solute elements (Mg, Zn, Cu and Ag) and vacancies (Va) [73].

Configuration	Cluster	Binding energy [meV]	Cluster	Binding energy [meV]	Cluster	Binding energy [meV]
	a) Alloy Zn		b) Alloy Zn CuX		c) Alloy Zn CuX Ag	
X-X	Mg-Zn	40	Cu-Cu	60	Ag-Ag	120
	Zn-Zn	20	Mg-Zn	40	Mg-Ag	90
	Mg-Mg	20	Cu-Zn	30	Cu-Ag	80
Va-X	Va-Zn	50	Va-Zn	50	Va-Ag	110
	Va-Mg	10	Va-Cu	30	Va-Zn	50
			Va-Mg	10	Va-Cu	30
X-X-Va	Mg-Va/Zn	100	Cu-Va/Cu	100	Mg-Va/Ag	190
	Zn-Zn/Va	90	Mg-Va/Cu	100	Ag-Va/Ag	160
	Mg-Zn/Va	80	Mg-Va/Zn	100	Cu-Va/Ag	150

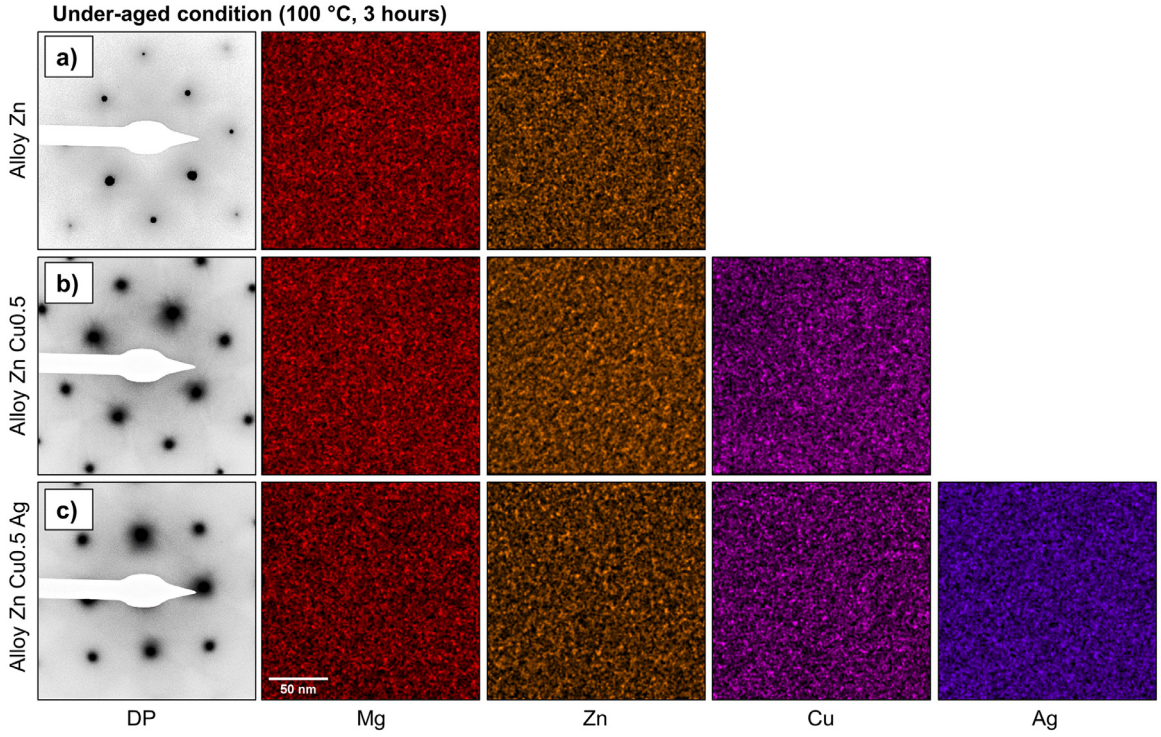

Fig. 9. DPs of the alloys and EDS mappings of the main alloying elements in Alloy Zn (a), Alloy Zn Cu0.5 (b) and Alloy Zn Cu0.5 Ag (c) in under-aged condition of double-step aging (100 °C/3 hours). The scale bar in the Mg mapping in (c) applies to all EDS mappings in (a), (b) and (c).

tachment of solutes shifting the hardening onset and peak hardness towards earlier aging times [43,45].

In peak-aged condition large, elongated T-phase precipitates are present in the matrix (Fig. 10a). Their number density is significantly smaller compared to single-step aging (Fig. 6a), which is attributed to the drastically increased diffusion at 175 °C and the resulting favored growth of large precipitates on the cost of small ones [60,61]. This effect is even more pronounced in the long-aged condition (Fig. 11a) coming along with a drastically decreased hardening ability (over-aging).

4.2. Effect of Cu on the aging response of Zn-enhanced EN AW-5182

The hardening response of the Zn-modified AlMg alloy is significantly boosted and accelerated by adding Cu. For single-step aging the hardening onset is shifted towards earlier aging times by changing the sharp hardness transition to a steady increase which starts immediately at the beginning of aging treatment. The boosting effect of Cu in Mg-containing alloys has been previously reported for 2xxx-series [63–65], 6xxx-series [66,67], 7xxx-series [68–70] alloys and Cu-added 5xxx-series alloys [19,21–24]. Particularly in AlCuMg and AlMgCu alloys this effect has been linked to Mg-Cu-cluster hardening, which represents the earliest stage of S-phase precipitation [SSSS ➔ Mg-Cu-clusters/GPB zones ➔ intermediate phase S'' ➔ intermediate phase S' ➔ equilibrium phase S-Al_2MgCu]. In light of the ongoing debate about the exact description of the precipitation sequence and the related crystal structures, we make no attempt to distinguish between the different evolution stages.

STEM investigations on the Cu-added alloys (especially Alloy Zn Cu0.5) in peak-aged and long-aged condition of single-step aging indicate that S-phase or its precursors are indeed present along with the T-phase (or its precursors). This has also been previously reported by several authors investigating comparable alloy compositions [40–43,45]. The fact that S-phase spots are very fainted and that Mg-Cu aggregates were not found by EDS measurements indicates a very low number density of these precipitates in the investigated alloy and condition resulting in an only marginal hardening contribution, which is attributed to the low total Cu content and its limited diffusivity at low temperatures [71].

After 3 hours of single-step aging at 125 “C (Fig. 5b) no extra reflection spots are present in the DP, which indicates that the hardness increase observed results from GPI-zones found in the corresponding BF images (Fig. 4b). Even though their composition was not assessed in the current study, APT results reported by Cao et al. [42] in a similar alloy in the under-aged state indicate that

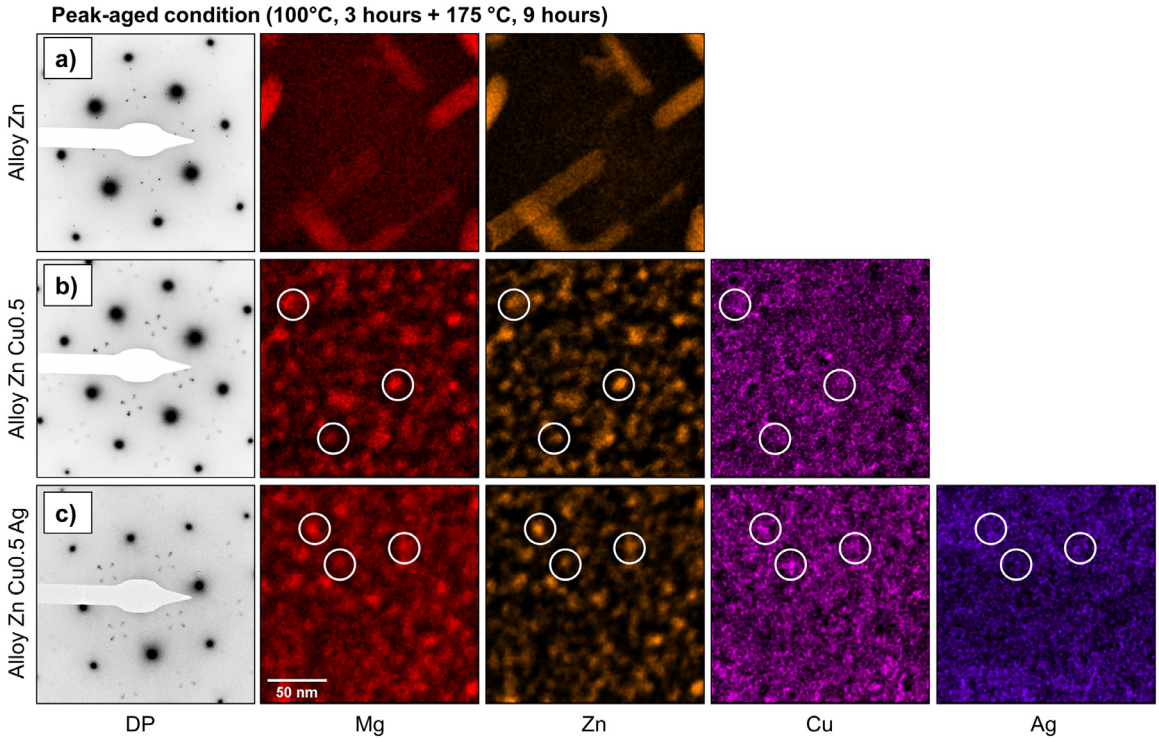

Fig. 10. DPs of the alloys and EDS mappings of the main alloying elements in Alloy Zn (a), Alloy Zn Cu0.5 (b) and Alloy Zn Cu0.5 Ag (c) in peak-aged condition of double-step aging (100 °C/3 hours + 175 °C/9 hours). White circles indicate correlation of Mg and Zn. The scale bar in the Mg mapping in (c) applies to all EDS mappings in (a), (b) and (c).

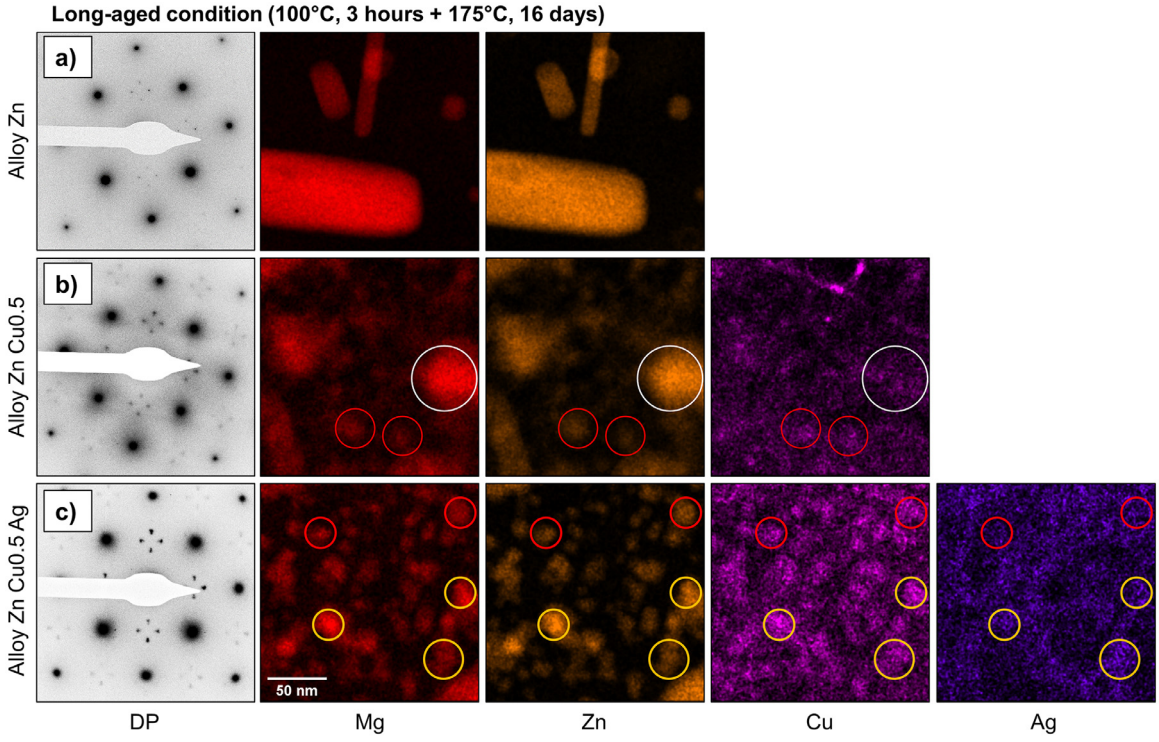

Fig. 11. DPs of the alloys and EDS mappings of the main alloying elements in Alloy Zn (a), Alloy Zn Cu0.5 (b) and Alloy Zn Cu0.5 Ag (c) in long-aged condition (100 °C/3 hours + 175 °C/16 days). White circles indicate correlation of only Mg and Zn, red circles indicate aggregation of Mg, Zn and Cu and orange circles indicated aggregates of Mg, Zn, Cu and Ag. The scale bar in the Mg mapping in (c) applies to all EDS mappings in (a), (b) and (c).

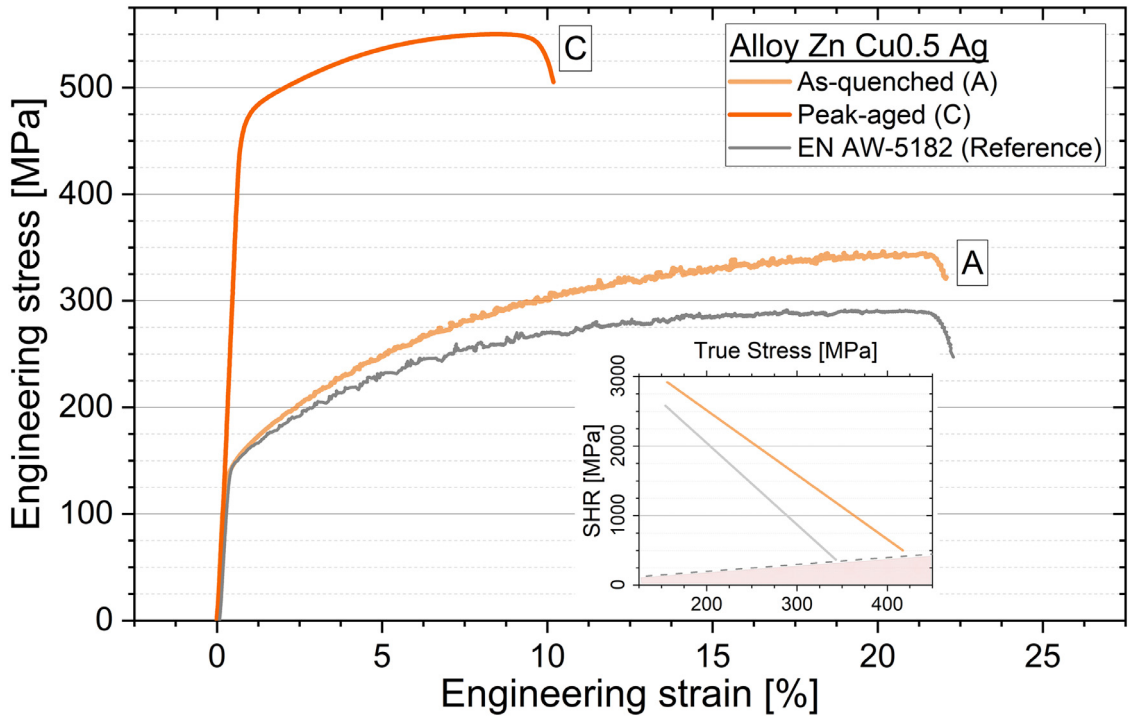

Fig. 12. Stress-strain curves of Alloy Zn Cu0.5 Ag in soft (A) and hard (C) temper and EN AW-5182 in its dedicated forming condition (gray curve). Inset: Kock-Mecking-plots [58] corresponding to Alloy Zn Cu0.5 Ag in soft temper (A) and EN AW-5182. The dashed gray line represents the Considère criterion.

GPI zones containing small but significant amounts of Cu were responsible for the early stage hardening. They concluded that Mg-Cu-clusters in great density might act as "nuclei" for the formation of hardening GPI zones which grow by gradual increase of Zn and gradual decrease of Mg and Cu with prolonged aging time [42].

Even though Zn and Cu exhibit similar attractive interaction energies with Mg atoms according to first principle calculations on solute pairs performed by Ogura et al. [72], the formation of Mg-Cu-clusters seems to be favored over Mg-Zn-clusters. This may be related to an atomic size effect and, therefore, to a minimization of the misfit strain between precursor and matrix because Mg atoms are larger by 12%, whereas Cu and Zn are smaller by 10% and 2.8%, respectively [41]. The beneficial effect of Cu was additionally proven by extended DFT calculations [73] in the Cu-added Al-Mg-Zn system (see Table 2b). Triplets of Cu-Va/Cu, Mg-Va/Cu and Mg-Va/Zn exhibit a significantly higher formation probability compared to solute pairs of Mg, Zn and Cu as well as to clusters in the Cu-free Al-Mg-Zn system (see Table 2a). As a result, the development of GPI-zones is enhanced by Cu-additions, which agrees well with our findings.

An additional explanation for the earlier hardening onset might be a decrease in activation energy for T-phase formation in combination with higher strengthening ability of Cu-containing GPI zones, as observed in 7xxx-series alloys [69].

Even though EDS mappings performed for Alloy Zn Cu0.5 reveal no distinct aggregation of Cu in the T-phase precipitates (white circles in Figs. 6b and 7b), their morphology has changed in the direction of a more circular shape, which may be favorable for inheriting a coherent relationship with the matrix as peak hardness was reached after longer aging time compared to Alloy Zn.

Applying a pre-aging treatment on the Cu-added alloys (especially Alloy Zn Cu0.5) peak hardness is shifted to much earlier aging times (9 hours instead of 9 days) upon aging in the second high-temperature stage similar to Alloy Zn. In contrast to the Cu-free alloy the peak hardness observed is significantly higher for Alloy Zn Cu0.5. This is attributed to the boosting effect of Cu on GPI-zone formation as explained above and results in a high number density of GPI-zones in under-aged condition (Fig. 8b). The slightly higher hardness after 3 hours of aging at 100 °C (double-step strategy) compared to aging at 125 °C (single-step strategy) is attributed preferred formation of solute aggregates at lower temperature as discussed in Section 4.1 [42,45,62].

In peak-aged condition of double-step aging the number density of T-phase precipitates in Alloy Zn Cu0.5 (Fig. 10b) exceeds the number density of Alloy Zn (Fig. 10a) drastically, resulting from the higher number of GPI-zones serving as nuclei at earlier stages.

The absence of S-phase reflection spots in the corresponding DP, the slightly higher number density and the indications of Cu-incorporation support the assumption of Cu-incorporation in the T-phase which might also explain the stronger hardening of these precipitates compared to the non-Cu-containing T-phase after single-step aging [42,43,45].

Similar to Alloy Zn the higher diffusivity of solutes in the high-temperature aging stage promotes undesired precipitate growth (Fig. 11b) resulting in a deterioration of hardness. It is worth emphasizing that precipitates with clear Cu-incorporations (red circles) do not coarsen as much as precipitates without Cu-incorporations (white circles) at this stage and a change of precipitate morphology with Cu addition is also evident (compare Fig. 11a and b). Both observations require additional research and won't be discussed here in detail due to the limited scope of this study but might be attributed to a decreased interfacial energy of Cu-containing precipitates inhibiting Ostwald ripening to some extent [60].

4.3. Effect of Ag on the aging response of Zn-and Cu-modified EN AW-5182

If Ag-doping is applied on all Zn-modified alloys independently of the Cu-content, the hardening onset is shifted to earlier aging times without affecting the hardening behavior (shape of the curve) and the peak hardness is distinctively increased for

single-step aging (Fig. 1), reaching a maximum of 166 HBW for Alloy Zn Cu0.5 Ag. Such peak aging generated a strength increase of 326 MPa, leading to a yield strength of 469 MPa (Fig. 12).

The stimulating effect of Ag on the precipitation process observed has been previously reported for other aluminum alloys and has been found to depend strongly on alloy composition. While additions of Ag in 7xxx-series alloys stimulate an existing precipitation sequence [29], they introduce new precipitate species in 2xxx-series [28,74,75] or enable aging hardening in usually non-heat treatable 5xxx-series alloys [76,77].

In the single-step, under-aged condition (3 h at 125 °C) a high number density of GPI-zones is evident in the corresponding BF image (Fig. 4c). The absence of extra reflection spots beside the matrix spots (DP in Fig. 5c) proofs that these precipitates have not developed a distinct crystal structure even though an even higher hardness increase was observed compared to that of Alloy Zn Cu0.5. We link the increased hardening to the higher number density of GPI-zones observed and their increased hardenability, which is favored by the addition of Ag. Similar effects have been reported in several studies of different alloy systems containing Mg [28,29,33,77–81] at early aging stages. According to first principle calculations by Sato et al. [82], Ag atoms exhibit an even stronger attractive interaction energy with Mg atoms compared to Cu and Zn atoms and, therefore, promote intensified clustering of Mg, Zn, Cu and Ag. Recent DFT calculations [73] shown in the Table 2c) support these findings (Mg-Va/Ag, Ag-Va/Ag and Cu-Va/Ag have a significantly higher formation probability compared to Ag-free clusters).

As a result, Ag-additions promote a larger density of nuclei, causing an increased hardening response. Because peak hardness was not shifted to shorter aging times, Ag additions seem to have no significant effect on the precipitation kinetics.

For Alloy Zn Cu0.5 Ag the high level of hardness in peak-aged (Fig. 6c) and long-aged (Fig. 7c) condition after single-step aging is caused by finely dispersed equiaxed T-phase or its precursors in a number density greater than that of the non-Ag-doped Alloy Zn Cu0.5, with the S-phase absent. The suppression of the S-phase may be related to the favored consumption of Cu atoms by early-stage clusters if Ag is present (see Cu-Va/Ag clusters in Table 2c) but could not be confirmed with the applied experimental methods [42,43,45].

While in peak-aged condition Mg-Zn-Ag aggregates (green circles in Fig. 6d) are present beside Mg-Zn aggregates (white circles in Fig. 6d) in Alloy Zn Cu0.5 Ag, additional aggregates of Mg, Zn, Ag and Cu are evident in long-aged condition (orange circles in Fig. 7d). The hardening phase may be therefore described as Cu- and Ag-incorporated T-phase [$Mg_{32}(Al,Zn,Cu,Ag)_{49}$] as also found by Suzuki et al. [34] and Vietz et al. [27]. Icosahedral quasi-crystals [36] or Z-phase precipitates [81] were not observed in this study. The lack of Cu-incorporation in peak-aged condition compared to its presence in long-aged condition is attributed to the limited diffusivity of Cu within the Al matrix compared to Ag at low temperatures and the significantly shorter aging time [71,83]. This supports the conclusion that T-phase composition is strongly linked to aging condition.

In under-aged condition of double-step aging a high number density of small GPI-zones is evident in the corresponding BF image (Fig. 8c) resulting from the combined effect of Cu and Ag on GPI-zone formation as explained above. In addition to the favored formation of precursors their increased binding energy might also contribute to their increased strengthening ability [52,69].

Upon subsequent high-temperature aging some of these precursors, which have not grown to a sufficient size during pre-aging, may initially dissolve (as indicated by the decline in hardness) while those with over-critical size grow and develop their full hardening potential [45].

The promoted GPI-zone formation by additions of Ag seems to add almost no extra benefit on peak hardness compared to Alloy Zn Cu0.5 if the current double-step aging treatment is applied. The microstructure of Alloy Zn Cu0.5 Ag consists of a high number of small, globular T-phase or it precursors (see DP in Fig. 10c). Similar to Alloy Zn Cu0.5 there are indications of Cu- and Ag-incorporations (white circles in Fig. 10c) but a clear aggregation could not be observed at this stage which is attributed to the relatively short aging time of 9 hours in the high-temperature aging stage [71,83].

With subsequent high-temperature aging (16 days at 175 °C) diffusivity of Cu and Ag is significantly enhanced and Cu-incorporated T-phase precipitates (red circles in Fig. 11c) are present beside Cu- and Ag-containing T-phase (orange circles in Fig. 11c). This observation and the absence of S-phase reflection spots [42,43,45] in the corresponding DPs after peak- (Fig. 10c) and long-aging (Fig. 11c) additionally support the assumption that Cu/Ag-containing T-precipitates [$Mg_{32}(Al,Zn,Cu,Ag)_{49}$] are the major hardening contributors in this system [27,31,34]. Similar to Alloy Zn Cu0.5 (Fig. 11b) hardening precipitates in Alloy Zn Cu0.5 Ag (Fig. 11c) have coarsened to a distinctively smaller extent compared to precipitates in Alloy Zn (Fig. 11a). The inhibiting effect of Cu on undesired precipitate growth (as already mentioned in Section 4.2) seems to be intensified if Ag is present. Even though the mechanism behind this observation is not clear at the moment, limited precipitate growth has been previously reported in several Ag-containing aluminum alloys [29,84–86].

4.4. Mechanical properties

To evaluate its potential for a commercial manufacturing process Alloy Zn Cu0.5 Ag was tensile tested in soft (condition A in Fig. 12) and peak-aged (condition C in Fig. 12) condition. Even though the alloy content is significantly greater than that of a commercial EN AW-5182, its formability in terms of uniform elongations has not deteriorated and strain hardening behavior is even increased in soft temper. This effect may be caused by the increased content of solutes in solid solution, as reported by Dorn et al. [87]. Interestingly, significant work hardening potential can still be found in the peak-aged state, leading from a yield strength of 469 MPa towards an ultimate tensile strength of 550 MPa and, therefore, reaching the area of commercial 7xxx-series alloys [88]. We assume that this is caused by remaining Mg in solid solution [4], which was not consumed by precipitate formation.

The PLC effect is also suppressed (partly in soft and fully in peak aged condition). This is assumed to result from initial clustering of Zn, Cu and Ag with Mg atoms upon quenching from solution heat, leading to a depletion of Mg in the matrix as reported by Ebenberger et al. [15,56].

5. Conclusions

This study investigated the effect of Cu and Ag additions on the aging behavior of Zn-modified AlMg alloys. The results can be summarized as follows:

- Adding Zn to a commercial EN AW-5182 alloy generates distinct age hardening potential by enabling the precipitation of lath-like T-$Mg_{32}(Al,Zn)_{49}$ and its precursors. Applying a double-step artificial aging treatment shifts the peak hardness to earlier aging times compared to single-step aging.
- Adding Cu to the Zn-modified AlMg alloy affects the peak hardness, which is primarily caused by equiaxed T-phase, only minor during single-step aging but shifts the hardness increase to earlier times by changing the hardening behavior in the direction of a steadier increase immediately after the beginning of

aging, which was found to result from a stimulating effect of Cu on GPI-zone formation. If low-temperature pre-aging is applied peak hardness in the high-temperature stage is shifted to earlier aging times and is significantly enhanced: This was caused by enhanced formation of GPI-zones during pre-aging, facilitating a higher density of hardening precipitates and ultimately leading to a higher hardness compared to the non-Cu-containing alloy.

- Doping with Ag shifts the hardening onset to even earlier single-step aging times by intensified formation of GPI-zones in high number density. Upon subsequent aging peak hardness results from finely dispersed T-phase precipitates in high number density inherited from early stage precursors. Pre-aging of Ag-doped alloys was found to be more beneficial for non-Cu-containing alloys because a significant number of GPI-zones is already present after the first aging step in Cu-containing alloys. Nevertheless, the time required for peak hardness is reached at significantly shorter total aging times.
- Tensile testing of the Zn-modified AlMg alloy containing both Cu and Ag indicates beneficial stretch-formability in soft temper (reduced stretcher straining, good uniform elongation, high work hardening) and high strength in peak-aged condition due to hardening by T-phase or its precursors.

According to the findings presented, AlMg alloys modified with Zn, Cu and Ag offer great potential for application in the transport sector, also via the use of a single-alloy concept.

Data availability

The raw/processed data required to reproduce these findings cannot be shared at this time as the data also forms part of an ongoing study.

Declaration of Competing Interest

None

CRediT authorship contribution statement

Lukas Stemper: Conceptualization, Methodology, Investigation, Visualization, Writing - original draft. **Matheus A. Tunes:** Investigation, Visualization, Writing - review & editing. **Paul Oberhauser:** Writing - review & editing. **Peter J. Uggowitzer:** Conceptualization, Supervision, Writing - review & editing. **Stefan Pogatscher:** Project administration, Conceptualization, Supervision, Writing - review & editing.

Acknowledgements

Financial support by the Christian Doppler Research Association, the Austrian Federal Ministry for Digital and Economic Affairs, the National Foundation for Research, Technology and Development and AMAG rolling GmbH is gratefully acknowledged. MAT and SP are grateful for the European Research Council (ERC) excellent science grant “TRANSDESIGN” through the Horizon 2020 program under contract 757961 and for financial support from the Austrian Research Promotion Agency (FFG) within project 3DnanoAnalytics (FFG-No. 858040). LS and MAT are grateful to Dr Thomas M. Kremmer (MUL) for useful discussions on T- and S-phase crystallographic identification within the TEM.

References

[1] J. Hirsch, Recent development in aluminium for automotive applications, Trans. Nonferrous Metals Soc. China 24 (2014) 1995–2002.
[2] J. Hirsch, Aluminium in Innovative Light-Weight Car Design, Mater. Trans. 52 (2011) 818–824.
[3] D. Raabe, C.C. Tasan, E.A. Olivetti, Strategies for improving the sustainability of structural metals, Nature 575 (2019) 64–74.
[4] F. Ostermann, Anwendungstechnologie Aluminium, Springer Berlin Heidelberg, Berlin/Heidelberg, 2014.
[5] W. Sylwestrowicz, E.O. Hall, The deformation and ageing of mild steel, Proc. Phys. Soc. Section B 64 (1951) 495.
[6] A. Portevin, F. Le Chatelier, Sur un phénomène observé lors de l'essai de traction d'alliages en cours de transformation, Comptes Rendus de l'Académie des Sci. 176 (1923) 507–510.
[7] R.E. Sanders, S.F. Baumann, H.C. Stumpf, Non-heat-treatable aluminum alloys, Aluminum Alloys: Their Physical and Mechanical Properties, 3, 1986, pp. 1441–1484.
[8] H.-P. Falkenstein, W. Gruhl, Forming behavior of aluminum, Bander-Bleche-Rohre 19 (1978) 265–268.
[9] A. Bigot, P. Auger, S. Chambreland, D. Blavette, A. Reeves, Atomic scale imaging and analysis of T' Precipitates in Al-Mg-Zn Alloys, Microsc. Microanal. Microstruct 8 (1997) 103–113.
[10] C. Meng, Di Zhang, H. Cui, L. Zhuang, J. Zhang, Mechanical properties, intergranular corrosion behavior and microstructure of Zn modified Al–Mg alloys, J. Alloys Compd. 617 (2014) 925–932.
[11] K. Matsumoto, Y. Aruga, H. Tsuneishi, H. Iwai, M. Mizuno, H. Araki, Effects of Zn addition and aging condition on serrated flow in Al-Mg Alloys, Mater. Sci. Forum 794-796 (2014) 483–488.
[12] J. Yun, S. Kang, S. Lee, D. Bae, Development of heat-treatable Al-5Mg alloy sheets with the addition of Zn, Mater. Sci. Eng. A 744 (2019) 21–27.
[13] X.B. Yang, J.H. Chen, J.Z. Liu, F. Qin, J. Xie, C.L. Wu, A high-strength AlZnMg alloy hardened by the T-phase precipitates, J. Alloys Compd. 610 (2014) 69–73.
[14] K. Matsumoto, Y. Aruga, H. Tsuneishi, H. Iwai, M. Mizuno, H. Araki, Effects of Precipitation State on Serrated Flow in Al-Mg(-Zn) Alloys, Mater. Trans. 57 (2016) 1101–1108.
[15] P. Ebenberger, P.J. Uggowitzer, B. Gerold, S. Pogatscher, Effect of compositional and processing variations in New 5182-Type AlMgMn alloys on mechanical properties and deformation surface quality, Materials (Basel, Switzerland) 12 (2019).
[16] M.C. Carroll, P.I. Gouma, M.J. Mills, G.S. Daehn, B.R. Dunbar, Effects of Zn additions on the grain boundary precipitation and corrosion of Al-5083, Scr. Mater. 42 (2000) 335–340.
[17] C.-Y. Meng, Di Zhang, P.-P. Liu, L.-Z. Zhuang, J.-s. Zhang, Microstructure characterization in a sensitized Al–Mg–Mn–Zn alloy, Rare Met. 37 (2015) 129–135.
[18] J.-w. Zhao, B.-h. Luo, K.-j. He, Z.-h. Bai, B. Li, W. Chen, Effects of minor Zn content on microstructure and corrosion properties of Al—Mg alloy, J. Cent. South Univ. 23 (2016) 3051–3059.
[19] O. Engler, C.D. Marioara, T. Hentschel, H.-J. Brinkman, Influence of copper additions on materials properties and corrosion behaviour of Al–Mg alloy shee, J. Alloys Compd. 710 (2017) 650–662.
[20] M. Hino, S. Koga, S. Oie, M. Yanagawa, Properties of Al-Mg Based Alloys for Automobile Body Panel, Kobelco Technol. Rev. 11 (1991) 1–5.
[21] A. Alil, M. Popović, T. Radetić, M. Zrilić, E. Romhanji, Influence of annealing temperature on the baking response and corrosion properties of an Al–4.6wt% Mg alloy with 0.54wt% Cu, J. Alloys Compd. 625 (2015) 76–84.
[22] S. Medrano, H. Zhao, F. de Geuser, B. Gault, L.T. Stephenson, A. Deschamps, D. Ponge, et al., Cluster hardening in Al-3Mg triggered by small Cu additions, Acta Mater. 161 (2018) 12–20.
[23] P. Ratchev, B. Verlinden, P. de Smet, P. van Houtte, Precipitation hardening of an Al–4.2wt% Mg–0.6wt% Cu alloy, Acta Mater. (1998) 3523–3533.
[24] P. Ratchev, B. Verlinden, P. de Smet, P. van Houtte, Artificial Ageing of Al–Mg–Cu Alloys, Mater. Trans. (1999) 34–41.
[25] L. Kovarik, P.I. Gouma, C. Kisielowski, S.A. Court, M.J. Mills, Decomposition of an Al–Mg–Cu alloy—A high resolution transmission electron microscopy investigation, Mater. Sci. Eng., A 387-389 (2004) 326–330.
[26] A. Charai, T. Walther, C. Alfonso, A.-.M. Zahra, C.Y. Zahra, Coexistence of clusters, GPB zones, S″-, S′- and S-phases in an Al–0.9% Cu–1.4% Mg alloy, Acta Mater. 48 (2000) 2751–2764.
[27] J.T. Vietz, I.J. Polmear, The influence of small additions of silver on the ageing of aluminium alloys, J. Inst. Metals 94 (1966) 410–419.
[28] S.P. Ringer, T. Sakurai, I.J. Polmear, Origins of hardening in aged Al-Cu-Mg-(Ag) alloys, Acta Mater. 45 (1997) 3731–3744.
[29] S.K. Maloney, K. Hono, I.J. Polmear, S.P. Ringer, The Effects of a Trace Addition of Silver Upon Elevated Temperature Ageing of an Al-Zn-Mg alloy, Micron (Oxford, England 1993), 2001, pp. 741–747.
[30] T. Ogura, T. Otani, A. Hirose, T. Sato, Improvement of strength and ductility of an Al–Zn–Mg alloy by controlling grain size and precipitate microstructure with Mn and Ag addition, Mater. Sci. Eng., A 580 (2013) 288–293.
[31] Q. Zhu, L. Cao, X. Wu, Y. Zou, M.J. Couper, Effect of Ag on age-hardening response of Al-Zn-Mg-Cu alloys, Mater. Sci. Eng.: A 754 (2019) 265–268.
[32] M. Kubota, J.F. Nie, B.C. Muddle, Characterisation of Quasicrystalline Particles in an Isothermally Aged Al–10Mg–0.5Ag (mass%) Alloy, Mater. Trans. 46 (2005) 1278–1287.
[33] M. Kubota, B.C. Muddle, Effect of Trace Additions of Ag on Precipitation in Al–Mg Alloys, Mater. Trans. 46 (2005) 2968–2974.
[34] Y. Suzuki, A. Hibino, T. Muramatsu, S. Hirosawa, T. Sato, Bake-hardenability of Al-Mg-Cu-X (Ag,Zn,Si) alloy sheets, Mater. Forum 28 (2004) 258–263.

[35] M. Mihara, E. Kobayashi, T. Sato, Rapid Age-Hardening Behavior of Al–Mg–Cu (–Ag) Alloys and Incubation Stage in the Low-Temperature Aging, Mater. Trans. 54 (2013) 1898–1904.
[36] M. Mihara, C.D. Marioara, S.J. Andersen, R. Holmestad, E. Kobayashi, T. Sato, Precipitation in an Al–Mg–Cu alloy and the effect of a low amount of Ag, Mater. Sci. Eng., A 658 (2016) 91–98.
[37] M.C. Carroll, P.I. Gouma, G.S. Daehn, M.J. Mills, Effects of minor Cu additions on a Zn-modified Al-5083 alloy, Mater. Sci. Eng., A 319-321 (2001) 425–428.
[38] M.C. Carroll, R.G. Buchheit, G.S. Daehn, M.J. Mills, Optimum Trace Copper Levels for SCC Resistance in a Zn-Modified Al-5083 Alloy, Mater. Sci. Forum 396-402 (2002) 1443–1448.
[39] C. Meng, Di Zhang, L. Zhuang, J. Zhang, Correlations between stress corrosion cracking, grain boundary precipitates and Zn content of Al–Mg–Zn alloys, J. Alloys Compd. 655 (2016) 178–187.
[40] C. Cao, Di Zhang, Z. He, L. Zhuang, J. Zhang, Enhanced and accelerated age hardening response of Al-5.2Mg-0.45Cu (wt%) alloy with Zn addition, Mater. Sci. Eng., A 666 (2016) 34–42.
[41] C. Cao, Di Zhang, X. Wang, Q. Ma, L. Zhuang, J. Zhang, Effects of Cu addition on the precipitation hardening response and intergranular corrosion of Al-5.2Mg-2.0Zn (wt.%) alloy, Mater. Charact. 122 (2016) 177–182.
[42] C. Cao, Di Zhang, L. Zhuang, J. Zhang, Improved age-hardening response and altered precipitation behavior of Al-5.2Mg-0.45Cu-2.0Zn (wt%) alloy with pre-aging treatment, J. Alloys Compd. 691 (2017) 40–43.
[43] S. Hou, P. Liu, Di Zhang, J. Zhang, L. Zhuang, Precipitation hardening behavior and microstructure evolution of Al–5.1 Mg–0.15Cu alloy with 3.0Zn (wt%) addition, J. Mater. Sci. 53 (2018) 3846–3861.
[44] S. Hou, Di Zhang, Q. Ding, J. Zhang, L. Zhuang, Solute clustering and precipitation of Al-5.1Mg-0.15Cu-xZn alloy, Mater. Sci. Eng., A 759 (2019) 465–478.
[45] L. Stemper, B. Mitas, T. Kremmer, S. Otterbach, P.J. Uggowitzer, S. Pogatscher, Age-hardening of high pressure die casting AlMg alloys with Zn and combined Zn and Cu additions, Mater. Des. 181 (2019) 107927.
[46] F. Schmid, L. Stemper, S. Pogatscher, T. Ebner, Industry-oriented sample preparation of 6xxx and 5xxx aluminum alloys in laboratory scale, in: GDMB (Ed.), EMC 2019: Optimum utilization of resources and recycling for a sustainable solution, 2019.
[47] S.-.L. Chen, S. Daniel, F. Zhang, Y.A. Chang, X.-.Y. Yan, F.-.Y. Xie, R. Schmid-Fetzer et al., The PANDAT software package and its applications. database: PandatAl2018_TH, 2002.
[48] C.W. Bale, E. Bélisle, P. Chartrand, S.A. Decterov, G. Eriksson, A.E. Gheribi, K. Hack, FactSage thermochemical software and databases, 2010–2016: Thermochemical Software and Databases, Calphad 54 (2016) 35–53.
[49] P. Villars, K. Cenzual, Mg32(Al,Zn)49 (Mg32Zn31.9Al17.1) Crystal Structure: Datasheet from “PAULING FILE Multinaries Edition - 2012” in SpringerMaterials, Springer-Verlag Berlin Heidelberg & Material Phases Data System (MPDS), Switzerland & National Institute for Materials Science (NIMS), Japan. materials.springer.com/isp/crystallographic/docs/sd_1252007.
[50] G. Bergman, J.L.T. Waugh, L. Pauling, The crystal structure of the metallic phase Mg32(Al, Zn)49, Acta Cryst. 10 (1957) 254–259.
[51] L. Kovarik, M.K. Miller, S.A. Court, M.J. Mills, Origin of the modified orientation relationship for S(S′′)-phase in Al–Mg–Cu alloys, Acta Mater. 54 (2006) 1731–1740.
[52] H. Löffler, I. Kovcs, J. Lendvai, Decomposition processes in Al-Zn-Mg alloys, J. Mater. Sci. 18 (1983) 2215–2240.
[53] C.B. Carter, D.B. Williams (Eds.), Transmission Electron Microscopy: Diffraction, Imaging, and Spectrometry, Springer International Publishing, Cham, s.l., 2016.
[54] M. von Heimendahl, Electron Microscopy of Materials: An Introduction, Acad. Press, New York, NY, 1980.
[55] S.R.K. Malladi, F.D. Tichelaar, Q. Xu, M.Y. Wu, H. Terryn, J.M.C. Mol, F. Hannour, et al., Quasi in situ analytical TEM to investigate electrochemically induced microstructural changes in alloys: AA2024-T3 as an example, Corros. Sci. 69 (2013) 221–225.
[56] P. Ebenberger, P.J. Uggowitzer, S. Kirnstötter, B. Gerold, S. Zaefferer, S. Pogatscher, Processing-controlled suppression of Lüders elongation in AlMgMn alloys, Scr. Mater. 166 (2019) 64–67.
[57] B. Gruber, F. Grabner, G. Falkinger, A. Schökel, F. Spieckermann, P.J. Uggowitzer, S. Pogatscher, Room temperature recovery of cryogenically deformed aluminium alloys, Mater. Des. 193 (2020) 108819.
[58] H. Mecking, U.F. Kocks, Kinetics of flow and strain-hardening, Acta Metall. 29 (1981) 1865–1875.
[59] G.I. Taylor, The mechanism of plastic deformation of crystals, Proc. R. Soc. Lond. A 145 (1934) 362–387.
[60] D.A. Porter, K.E. Easterling, M.Y. Sherif, Phase Transformations in Metals and Alloys, CRC Press, Boca Raton, FL, 2009.
[61] N. Afify, A.-.F. Gaber, G. Abbady, Fine scale precipitates in Al-Mg-Zn alloys after various aging temperatures, MSA 02 (2011) 427–434.
[62] H. Inoue, T. Sato, Y. Kojima, T. Takahashi, The Temperature Limit for GP Zone Formation in an Al-Zn-Mg Alloy, Metall. Mat. Trans. A 12 (1981) 1429–1434.
[63] S.P. Ringer, K. Hono, T. Skurai, I.J. Polmear, Cluster hardening in an aged Al-Cu-Mg alloy, Scr. Mater. (1997) 517–521.
[64] R.K.W. Marceau, G. Sha, R. Ferragut, A. Dupasquier, S.P. Ringer, Solute clustering in Al–Cu–Mg alloys during the early stages of elevated temperature ageing, Acta Mater. 58 (2010) 4923–4939.
[65] R. Ivanov, A. Deschamps, F. de Geuser, Clustering kinetics during natural ageing of Al-Cu based alloys with (Mg, Li) additions, Acta Mater. 157 (2018) 186–195.
[66] T. Saito, C.D. Marioara, J. Røyset, R. Holmestad, Effect of Low Cu Addition and Thermo-Mechanical History on Precipitation in Al-Mg-Si Alloys, MSF 794-796 (2014) 1014–1019.
[67] J.-.H. Kim, H. Tezuka, E. Kobayashi, T. Sato, Effects of Cu and Ag Addition on Nanocluster Formation Behavior in Al-Mg-Si Alloys, Korean J. Mater. Res. 22 (2012) 329–334.
[68] N.Q. Chinh, J. Lendvai, D.H. Ping, K. Hono, The effect of Cu on mechanical and precipitation properties of Al–Zn–Mg alloys, J. Alloys Compd. 378 (2004) 52–60.
[69] A. Deschamps, Y. Bréchet, F. Livet, Influence of copper addition on precipitation kinetics and hardening in Al–Zn–Mg alloy, Mater. Sci. Technol. 15 (2013) 993–1000.
[70] P.V. Liddicoat, T. Honma, L.T. Stephenson, S.P. Ringer, Evolution of Nanostructure during the Early Stages of Ageing in Al-Zn-Mg-Cu Alloys, MSF 519-521 (2006) 555–560.
[71] Y. Du, Y.A. Chang, B. Huang, W. Gong, Z. Jin, H. Xu, Z. Yuan, et al., Diffusion coefficients of some solutes in fcc and liquid Al: critical evaluation and correlation, Mater. Sci. Eng., A 363 (2003) 140–151.
[72] T. Ogura, S. Hirosawa, A. Cerezo, T. Sato, Atom probe tomography of nanoscale microstructures within precipitate free zones in Al–Zn–Mg(–Ag) alloys, Acta Mater. 58 (2010) 5714–5723.
[73] J. Peng, S. Bahl, A. Shyam, J.A. Haynes, D. Shin, Solute-Vacancy Clustering in Aluminum (2020) arXiv:2004.01931v1.
[74] L. Reich, M. Murayama, K. Hono, Evolution of Ω phase in an Al–Cu–Mg–Ag alloy—A three-dimensional atom probe study, Acta Mater. 46 (1998) 6053–6062.
[75] S. Hirosawa, T. Sato, A. Kamio, Effects of Mg addition on the kinetics of low-temperature precipitation in Al–Li–Cu–Ag–Zr alloys, Mater. Sci. Eng., A 242 (1998) 195–201.
[76] I.J. Polmear, K.R. SARGANT, Enhanced Age-hardening in Aluminium–Magnesium Alloys, Nature 200 (1963) 669–670.
[77] I.J. Polmear, Role of Trace Elements in Aged Aluminium-Alloys, Mater. Sci. Forum 13-14 (1987) 195–214.
[78] E. Gumbmann, F. de Geuser, C. Sigli, A. Deschamps, Influence of Mg, Ag and Zn minor solute additions on the precipitation kinetics and strengthening of an Al-Cu-Li alloy, Acta Mater. 133 (2017) 172–185.
[79] S. Bai, X. Yi, Z. Liu, J. Wang, J. Zhao, P. Ying, The influence of preaging on the strength and precipitation behavior of a deformed Al-Cu-Mg-Ag alloy, J. Alloys Compd. 764 (2018) 62–72.
[80] C. Guo, H. Zhang, Z. Wu, D. Wang, B. Li, J. Cui, Effects of Ag on the age hardening response and intergranular corrosion resistance of Al-Mg alloys, Mater. Charact. 147 (2019) 84–92.
[81] S. Hirosawa, T. Omura, T. Sato, Y. Suzuki, Effects of Ag addition on age-hardening and nano-scale precipitate microstructures of an Al-3%Mg-1%Cu alloy, J. Jpn. Inst. Light Metals 56 (2006) 673–679.
[82] T. Sato, S. Hirosawa, K. Hirose, T. Maeguchi, Roles of microalloying elements on the cluster formation in the initial stage of phase decomposition of Al-based alloys, Metall. Mater. Trans. A 34 (2003) 2745–2755.
[83] T. Takahashi, K. Hisayuki, T. Yamane, Y. Minamino, Quaternary Diffusion in the α Solid Solutions of Al-Zn-Mg-Ag Alloys, DDF 194-199 (2001) 235–240.
[84] C.R. Hutchinson, X. Fan, S.J. Pennycook, G.J. Shiflet, On the origin of the high coarsening resistance of Ω plates in Al–Cu–Mg–Ag Alloys, Acta Mater. 49 (2001) 2827–2841.
[85] A. Ghosh, M. Ghosh, G. Shankar, On the role of precipitates in controlling microstructure and mechanical properties of Ag and Sn added 7075 alloys during artificial ageing, Mater. Sci. Eng.: A 738 (2018) 399–411.
[86] J. Li, Z. An, F.S. Hage, H. Wang, P. Xie, S. Jin, Q.M. Ramasse, et al., Solute clustering and precipitation in an Al–Cu–Mg–Ag–Si model alloy, Mater. Sci. Eng.: A 760 (2019) 366–376.
[87] J.E. Dorn, P. Pietrokowsky, T.E. Tietz, The effect of alloying elements on the plastic properties of aluminum alloys, JOM 2 (1950) 933–943.
[88] Y.-.S. Lee, D.-.H. Koh, H.-.W. Kim, Y.-.S. Ahn, Improved bake-hardening response of Al-Zn-Mg-Cu alloy through pre-aging treatment, Scr. Mater. 147 (2018) 45–49.